A year-long evaluation of a wind-farm parameterisation in HARMONIE-AROME

Bart van Stratum[1,2], Natalie Theeuwes[1*], Jan Barkmeijer[1], Bert van Ulft[1], Ine Wijnant[1]

[1]Royal Netherlands Meteorological Institute (KNMI), de Bilt, The Netherlands
[2]Department of Meteorology and Air Quality, Wageningen University, Wageningen, The Netherlands

Key Points:

- In this study a wind-farm parameterisation is implemented in the numerical weather prediction model HARMONIE-AROME.
- A model evaluation of a full year reveals the wind-farm parameterisation greatly improves wind-speed forecasts close to offshore wind farms.
- The presence of wind farms in the model also alters temperature and humidity profiles due to the enhanced turbulent mixing by the turbines.

Corresponding author: Natalie Theeuwes, `natalie.theeuwes@knmi.nl`

Abstract

The need to mitigate climate change will boost the demand for renewable energy and lead to more wind turbines both on- and onshore. In the near future, the effect these wind farms have on the atmosphere can no longer be neglected. In numerical weather prediction models wind-farm parameterisations (WFP) can be used to model the effect of wind farms on the atmosphere. There are different modelling approaches, but the parameterisation developed by Fitch et al. (2012) is most used in previous studies. It models the wind farm as a momentum sink and a source of power production and turbulent kinetic energy. In this paper, we have implemented the Fitch et al. (2012) WFP into HARMONIE-AROME, the numerical weather prediction model that is currently used by at least 11 national weather services in Europe. We used HARMONIE-AROME to make year-long simulations for 2016 with and without the WFP. The results were extensively evaluated using lidar, tower and flight measurements at several locations near wind farms. Including the WFP greatly reduces the model bias for wind speed near offshore wind farms. Wind farms not only affect wind, but also temperature and humidity, especially during stable atmospheric conditions: the enhanced mixing caused by the wind turbines reduces the stratification of temperature and humidity. Including the WFP in HARMONIE-AROME results in a more realistic representation of the atmosphere near wind farms and makes it a more future-proof model for weather forecasting.

Plain Language Summary

Wind power production is steadily increasing. Wind farms are growing both in number and size, while weather models evolve to higher resolutions. This means that the effect of wind farms can no longer be ignored by weather prediction models. Wind farms essentially decelerate the wind (blockage and wake effects) and increase turbulence, indirectly influencing temperature and humidity. In this study, we have included a widely used wind-farm parameterisation in the operational weather prediction model. The model is evaluated using various datasets, e.g. power production data, floating lidar measurements, and anemometer measurements from a tower. The inclusion of the wind-farm parameterisation improves the wind forecasts near wind farms, also improving the estimate in power production. In addition, we are able to model the effects of wind farms on the near-surface temperature and humidity.

1 Introduction

Offshore wind power production in the European Union (EU) and specifically the North-Sea region is steadily increasing: the Dutch offshore capacity is expected to grow from ±1 GW in 2019 to ±11.5 GW in 2030, as part of a total expected increase to ±70 GW in the entire EU (WindEurope, 2017). Wind turbines produce electric energy by extracting kinetic energy from the atmosphere, thereby decelerating (and agitating) the air. This typically results in a downstream decrease in wind speed and increase in turbulence (e.g. Baidya Roy & Traiteur, 2010; Fitch et al., 2012). As wind farms grow – both in size and number – the impact on weather and climate is expected to become more significant, requiring an adaptation of mesoscale models like HARMONIE-AROME (hereafter: HARMONIE) to account for the influence of wind farms on the local and regional meteorological conditions.

There are several ways in which the effects of wind turbines on the atmosphere can be parameterised in mesoscale models (Fischereit et al., 2021). The implicit – imposing an additional roughness to implicitly model the effect of wind turbines on the atmospheric flow – or explicit, explicitly solving the momentum sink and enhanced turbulence production due to the presence of wind turbines. In the last two decades several explicit parameterisations have been developed (e.g. Fitch et al., 2012; Abkar & Porté-Agel, 2015; Volker et al., 2015). The most commonly used and evaluated parameterisation is the Fitch et al. (2012) model implemented in the Weather Research and Forecasting (WRF) model (Skamarock et al., 2019).

In this study, we implemented the wind turbine parameterisation from Fitch et al. (2012) in HARMONIE. In the presence of wind turbines, this parameterisation adds an elevated drag term to the atmosphere, which locally decelerates the flow. The kinetic energy that is extracted from the atmosphere, but not converted into electric power, is used as a source term for turbulence kinetic energy (TKE).

HARMONIE with and without the newly-implemented wind-farm parameterisation is evaluated using doppler lidar and tower measurements over the North Sea over a period of one full year (January up to and including December 2016), instead of evaluating case studies as done in most evaluations of wind-farm parameterisations (e.g. Lee & Lundquist, 2017; Wu et al., 2022). During the full year, the parameterisation is evaluated for all seasons with varying wind directions and atmospheric stabilities. In 2016,

measurements were available from two floating lidars in the Borssele wind farm zone (off the Belgian coast), one ground-based lidar in the Westermost Rough wind farm (off the east-coast of the UK), cup-anemometer measurements on the FINO1 tower near the Alpha Ventus wind farm (north of the Netherlands) and aircraft measurements (off the north-west German coast). Since all these measurements are in or near existing wind farms, they are ideal for evaluating the newly implemented wind-farm parameterisation. The spatial impact of the wind farms on the wind fields is evaluated using dedicated flight campaigns (Lampert, Bärfuss, et al., 2020). The consequence of the WFP on power production is evaluated using Belgian transmission system operator (TSO) data. Moreover, the year-long experiment allowed us to quantify the impact of the offshore wind farms on the offshore and coastal meteorological conditions.

2 HARMONIE-AROME

The wind-farm parameterisation is implemented in HARMONIE-AROME (cycle 40h1), a non-hydrostatic model developed by the HIRLAM-C consortium, which is operationally used in at least 11 countries (Bengtsson et al., 2017). The model uses a semi-lagrangian scheme on an Eulerian grid. The turbulence scheme used was HARATU (de Rooy et al., 2021; Lenderink & Holtslag, 2004), which uses a prognostic equation for the turbulent kinetic energy (TKE), and shallow convection following de Rooy et al. (2021). Surface Externalisée (SURFEX) version 7.3 was used as a land surface model (Masson et al., 2013) with the land use classification from ECOCLIMAP II (Faroux et al., 2013). More details about the model physics can be found in Bengtsson et al. (2017) or www.hirlam.org.

3 Wind farm parameterisation

The wind-farm parameterisation of (Fitch et al., 2012) imposes an elevated momentum sink on the mean flow, where the drag (or thrust) of the individual turbine blades is modelled as a constant (but wind speed dependent) drag force across the area swept by the rotor blades. As the diameter of a wind turbine is about an order of magnitude smaller than the horizontal grid spacing in HARMONIE (currently: 2.5 km), the model accounts for the bulk influence of one or several wind turbines per grid point.

The wind turbine characteristics are defined by the geometry (hub-height z_{hub} and turbine radius r), the cut-in (V_{in}) and cut-out (V_{out}) wind speeds, and by the dimension-

less power (C_P) and thrust (C_T) coefficients. The latter two describe – as a function of wind speed V_hub at hub height – the fraction of kinetic energy that is extracted from the air (C_T), and the fraction that is converted into electrical energy (C_P). An example of typical C_P and C_T curves is provided in Fig. 1.

Given the thrust coefficient C_T, the thrust force of a turbine (the force opposite to the flow direction and drag force) is defined as:

$$\vec{F}_\mathrm{thrust} = -\frac{1}{2}\rho C_\mathrm{T}|\vec{V}|\vec{V}A_T, [\mathrm{N}] \tag{1}$$

where ρ is the air density (kg m^{-3}), $\vec{V} = (u, v)$ the horizontal wind vector (m s^{-1}), $|\vec{V}| = \sqrt{u^2 + v^2}$, and A_T is the rotor area (m^2). The rate of loss of kinetic energy (KE) then equals:

$$\left.\frac{\partial \mathrm{KE}}{\partial t}\right|_\mathrm{drag} = -\frac{1}{2}\rho C_\mathrm{T}|\vec{V}|^3 A_T.[\mathrm{J\,s^{-1}}] \tag{2}$$

In practise the rotor of a turbine intersects multiple model levels, and Eq 2 (and all equations in the remainder of this chapter) are solved for each model level k individually, replacing the rotor area A_T with the area intersected by the k-th model level, and the wind speed $|\vec{V}|$, and density ρ with values from the k-th model level, indicated where appropriate by a subscript k. As a result, the momentum sink (and TKE source) is elevated and height dependent.

In general, the total change in KE of a single grid cell with a volume $\Delta_k = (\Delta x \Delta y \Delta z_k)$ m^3 equals:

$$\left.\frac{\partial \mathrm{KE_k}}{\partial t}\right|_\mathrm{cell} = \frac{\partial}{\partial t}\left(\frac{1}{2}\rho_k|\vec{V_k}|^2\right)\Delta_k = \rho_k|\vec{V_k}|\frac{\partial|\vec{V_k}|}{\partial t}\Delta_k.[\mathrm{J\,s^{-1}}] \tag{3}$$

Combining Eqs 2 and 3, i.e. setting:

$$\left.\frac{\partial \mathrm{KE_k}}{\partial t}\right|_\mathrm{cell} = \left.\frac{\partial \mathrm{KE_k}}{\partial t}\right|_\mathrm{drag}, [\mathrm{J\,s^{-1}}] \tag{4}$$

results, after re-arranging, in an expression for the change in velocity with time:

$$\frac{\partial|\vec{V_k}|}{\partial t} = -\frac{1}{2}C_\mathrm{T}\ |\vec{V_k}|^2\ A_k\ \Delta_k^{-1}, [\mathrm{m\,s^{-2}}] \tag{5}$$

or, in component form:

$$\frac{\partial u_k}{\partial t} = -\frac{1}{2} C_{\mathrm{T}}\ u_k\ |\vec{V_k}|\ A_k\ \Delta_k^{-1}, [\mathrm{m\,s^{-2}}] \tag{6}$$

$$\frac{\partial v_k}{\partial t} = -\frac{1}{2} C_{\mathrm{T}}\ v_k\ |\vec{V_k}|\ A_k\ \Delta_k^{-1}.[\mathrm{m\,s^{-2}}] \tag{7}$$

The vertical velocity component is assumed to be unaffected by the wind turbines, and furthermore, drag by the wind turbine tower and nacelle is not included in the parameterisation. The energy that is extracted from the atmosphere, but not converted into electrical energy, is assumed to be converted into turbulence kinetic energy (TKE, per unit mass), i.e. $C_{\mathrm{TKE}} = C_{\mathrm{T}}$ - C_{P}, resulting in:

$$\frac{\partial \mathrm{TKE_k}}{\partial t} = \frac{1}{2} C_{\mathrm{TKE}}\ |\vec{V_k}|^3\ A_k\ \Delta_k^{-1}.[\mathrm{m^2\,s^{-2}\,s^{-1}}] \tag{8}$$

Finally, as a diagnostic quantity, the model outputs the electrical power produced by the wind turbines:

$$\mathrm{P} = \frac{1}{2} \rho C_{\mathrm{P}}\ A_T\ |\vec{V}_{\mathrm{hub}}|^3 [\mathrm{W}] \tag{9}$$

For a typical offshore wind farm, multiple wind turbines can occupy a single horizontal grid point. Instead of introducing a horizontal wind turbine density – like in (Fitch et al., 2012) – Eqs 6 to 9 are repeated for each individual turbine, allowing different turbine types in a single horizontal grid point. The total tendencies for the horizontal wind components and TKE are adjusted after the turbulence scheme is called and fed back to the model.

4 Experimental setup

HARMONIE used a 2000×2000 km^2 domain with 65 vertical levels, 2.5 km horizontal grid spacing, centred around 51.96°N, 4.9°E. The ERA5 reanalysis (Hersbach et al., 2020) is used for the lateral boundary conditions.

Two simulations were performed: (1) reference simulation without wind turbines, REF, and (2) with the wind-farm parameterisation modelling all offshore wind turbines

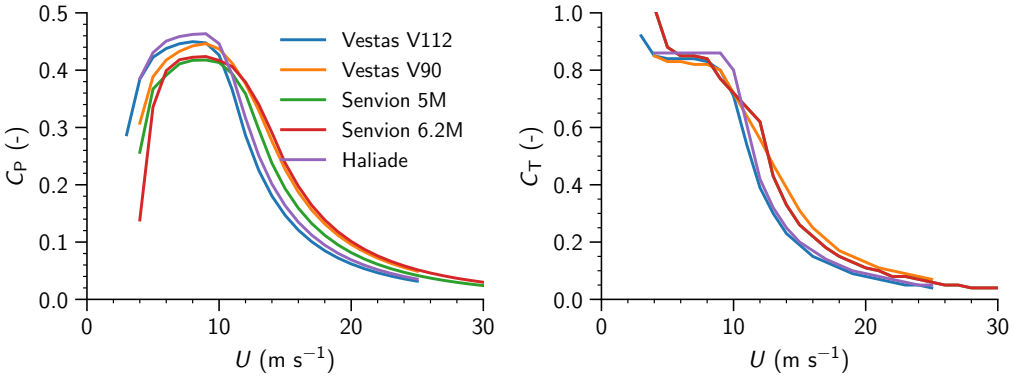

Figure 1. Power (C_P) and thrust (C_T) coefficients of the Belgian offshore wind turbines

present in the model domain in January 2016, WFP. The experiments are run from 01-01-2016 00 UTC to 01-01-2017 00 UTC. This period was chosen because of the availability of two floating lidars in the Borssele wind farm zone, directly north-east of the (Belgian) Northwind wind farm (Fig. 2). In addition, for this period there are tower measurements from the FINO1 platform, and lidar measurements from the Westermost Rough wind farm and flights through wind farm wakes in the German Bight (WIPAFF; Lampert, Bärfuss, et al., 2020).

The reference simulation was run for several years before the study period for the Dutch Offshore Wind Atlas (DOWA) project (Wijnant et al., 2019) and therefore had more than six years of spin-up. The WFP run was started 'warm' from the control experiment and had ten days of additional spin-up time. Both reanalysis simulations used 3D-VAR data assimilation (Fischer et al., 2005; Gustafsson et al., 2018) with a three-hour cycling time. In addition to conventional observations, Mode-S EHS aircraft measurements (e.g. de Haan, 2011, 2016) and Scatterometer (ASCAT) (Marseille & Stoffelen, 2017) were assimilated. In this study the 3-hour forecast is used as a proxy for the analysis.

For the Belgian and Dutch wind farms, the exact (individual) turbine coordinates are available, which could directly be used in the experiments. For the other offshore wind farms in the computational domain (Fig. 2), the available information was limited to the wind farm boundaries and the total number of turbines per wind farm. For these sites, the turbine coordinates were first chosen randomly within the wind farm boundary, and next distributed uniformly using an iterative repulsion method (Witkin & Heckbert, 2005).

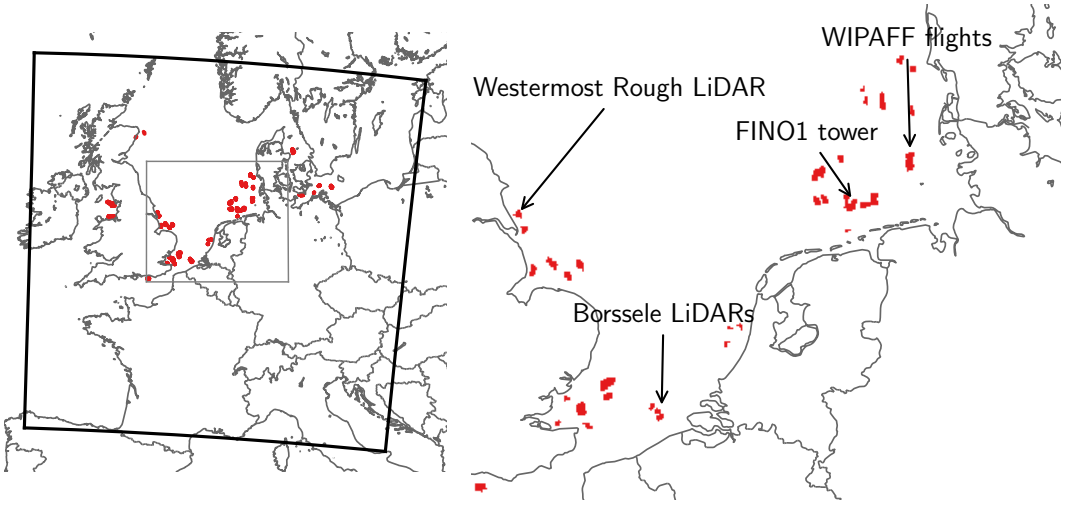

Figure 2. Overview of all (2.5×2.5 km) grid points with one or more wind turbines (red). Black arrows indicate the locations of measurements used for evaluation. In the left figure the black square indicates the model domain and the grey square the location of the right panel.

This random approach to determine the turbine coordinates can be justified by the fact that within the turbine parameterisation, all turbines are mapped to the nearest 2.5 km × 2.5 km grid point, making the exact turbine coordinates less important. The wind farm boundaries were obtained from the *The European Marine Observation and Data Network* (EMODnet; Martín Míguez et al., 2019).

The C_P and C_T curves were obtained from various sources, predominantly from windPRO input database (Acker & Chime, 2011). For a small number of turbines, no C_P and C_T curves were publicly available, those turbines have been replaced with either reference data from literature, or C_P and C_T curves from similar turbines. An overview is provided in Appendix A.

5 Measurements

5.1 Borssele Wind Lidars

For the wind resource assessment of the four wind farms in the Borssele wind farm zone (BWFZ), two short-range doppler lidars were deployed near the Belgian offshore wind farms. Fugro executed a Metocean campaign and did measurements for a number

of periods between June 2015 and February 2017. ZephIR 300S lidars were mounted on buoys with a bottom mooring weight at 51.707° N, 3.035° E (Fig. 3, lidar 1) and at 51.646° N, 2.951° E (Fig. 3, lidar 2). Lidar 1 (henceforth BWFZ1) measured for the longest period and there were sixteen measurement periods between June 2015 and February 2017 (Fig. 4a). This lidar is located 10 km northeast of the nearest wind turbine. Lidar 2 (henceforth BWFZ2) only measured during five periods and only between February and July 2016 (Fig. 4b). This lidar is closer to the Belgian wind farm zones, at 2 km from the nearest turbine (Fig. 3). At typical hub heights of about 90 m the uncertainty in floating lidar measurements for wind speeds between 4 and 15 m/s is between 3 and 4.5% (Duncan et al., 2019)

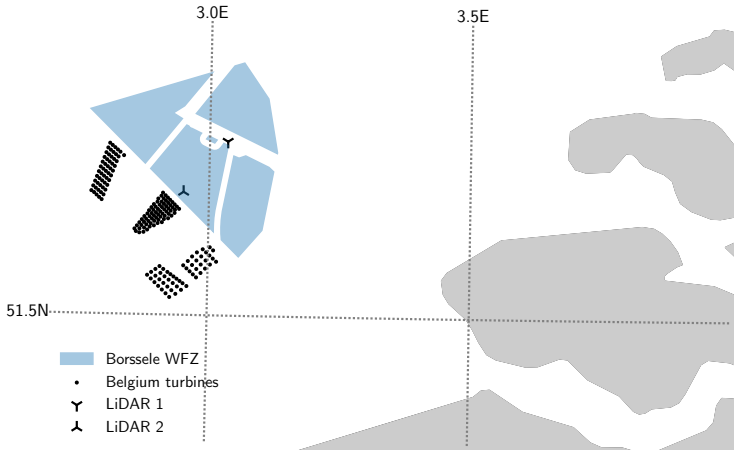

Figure 3. Setup of the Borssele wind lidars off the coast of Belgian and the Netherlands. The blue area are the planned wind farm zones, that started to be operational in 2020/2021.

5.2 FINO 1 Tower

The FINO 1 tower has been providing measurements since 2003 and is located in the North Sea at 54.015 ° N, 6.588 ° E, 50 km north of the Wadden island Borkum (Fig. 2). The water depth at this location is 30 m and the tower reaches a height of 103.7 m above Lowest Astronomical Tide (LAT). The first wind turbines were installed near FINO1 in November 2009 and the Alpha Ventus wind farm became fully operational in 2010. This means that wind measurements for wind directions between 15° to 165° (easterly winds) became disturbed by Alpha Ventus since November 2009. Borkum Riffgrund 1

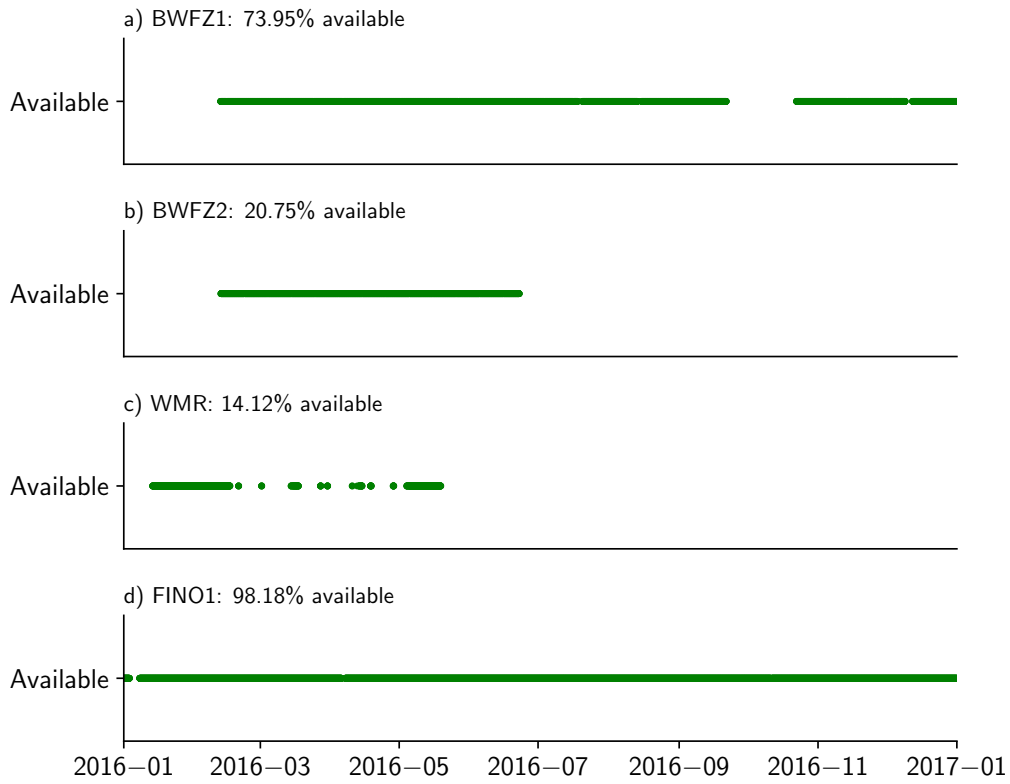

Figure 4. Availability of the measurements for the two lidars at the Borssele wind farm zone (a) BWFZ1 and (b) BWFZ2, (c) the Westermost Rough lidar (WMR) and (d) FINO 1.

to the south west has been fully operational since 2015, also disturbing the flow in 170° to 300° directions.

Here, we use the cup anomemeters to evaluate the model, since these measure at frequent height intervals (i.e. 34.1, 41.6, 51.6, 61.6, 71.6, 81.6, 91.6, 101.6). The cup anemometers are manufactured Vector Instruments Windspeed Ltd. type A100LK/PC3/WR with an accuracy of 1 %. The cup anemometers (for measuring wind speed) are on booms on the southeast side of the mast (towards 135–143°) and the wind vanes (for measuring wind direction) on booms on the opposite side of the mast. The wind speed measurements are corrected for wind mast effects using a measurement correction scheme called the UAM-correction methodWind direction measurements are not corrected. (i.e. Westerhellweg et al., 2010, 2012). Wind direction measurements are not corrected.

The FINO1 measurements are available for the whole of 2016 and only about 2.5 % of the data are missing (Fig. 4). Due to it's long-term measurements the tower has

been previously used to evaluate atmospheric models over the North Sea (e.g. Muñoz-Esparza et al., 2012; Wagner et al., 2019).

5.3 Westermost Rough Wind Lidar

On top of the Westermost Rough wind farm substation (Fig. 2), Ørsted operates a Leosphere WindCube scanning doppler lidar, providing wind speed measurements between 74 m to 324 m height. Westermost Rough wind farm is located off the coast of Yorkshire, UK. Unlike the Borssele lidars and FINO1 tower, this lidar is located in the centre of the wind farm (53.804° N, 0.132° N), and is therefore always disturbed by the wind turbines. The Westermost Rough (WMR) lidar became operational in mid-January 2016, but only has an overall availability of ∼14% (1.5 out of 12 months), which limits its usability.

5.4 WIPAFF

As part of the WInd PArk Far Field (WIPAFF) project (Platis et al., 2020), several measurements were taken around wind farms in the German Bight area (Fig. 2). In total 41 flights were carried out, of which 8 were in our current study period (6–10 September 2016). The aircraft measurements were carried out using the research aircraft Dornier 128. The aircraft is equiped with sensors measuring temperature, humidity, all wind components, and pressure at 100 Hz. This large dataset of spatial data is very valuable to evaluate mesoscale models with wind-farm parameterisations, and has been used previously to evaluate the Weather Research Forecasting model (WRF) (Platis et al., 2021). The measurements are described in detail by Lampert, Bärfuss, et al. (2020) and data are publicly available (Bärfuss et al., 2019).

For the purpose of this study we have only used one of the flights to evaluate the spatial representation of the wind farm wakes generated by HARMONIE. This flight took place on September 6 2016, between 12:13 and 15:20 downwind of Amrumbank West wind farm. During this day the average background wind speed was about 7 m s^{-1} from the south. Therefore the aircraft measurements were taken in a meandering pattern north of the wind farm at hub height (i.e. 90 m). Given the average speed of the plane was 54 m s^{-1} and to compare with the model data at a grid spacing of 2.5 km, a 60-second rolling average over the sonic anemometer data is performed.

5.5 Power production data

Belgium's high-voltage TSO, Elia, publishes the generated power by their various energy sources, including offshore wind farm power production in 15-minute intervals. Since in 2016 Belgium only had three offshore wind farms (Fig. 2 & 3), we are able to use their power generation data to evaluate the HARMONIE-modelled generated power. The total capacity of these offshore wind farms was 712.2 MW.

6 Evaluation

6.1 Offshore lidar and tower measurements

During the chosen period, all lidars had periods with missing data, as summarised in Fig. 4. For all statistical analyses in this section we use collocated data, i.e. missing data is removed (or masked) in the model dataset as well. In addition, there is no conditional sampling based on (e.g.) wind direction; all available measurements are always included in the statistics.

6.1.1 Borssele Wind Farm Zone (BWFZ) lidars

As shown in Fig. 3, both lidars were positioned north-east of the Belgian Northwind wind farm. With prevailing winds from the south-west, these lidar measurements are typically disturbed by the Belgian wind farms, making them ideal for assessing the impact of the wind turbines on the wind field, and the ability of the wind farm parametrisation to reproduce the disturbed wind field due to the wake effect of the wind farm.

Figure 5 shows the time averaged vertical wind speed profiles from the reference run (REF), the experiment with the wind-farm parameterisation (WFP), and the Borssele lidars. These are averaged profiles over the entire measurement period for both lidars and represent all different wind directions. However, over the duration of the measurement period of BWFZ1, the wind direction was southwesterly (180–270°) 42% of the time.

For both sites the reference simulation (without wind park parameterisation) overestimates the wind speed, which is most pronounced for lidar location number two, which is closest to the Belgian wind farms at 2 km distance from the nearest turbine. Enabling

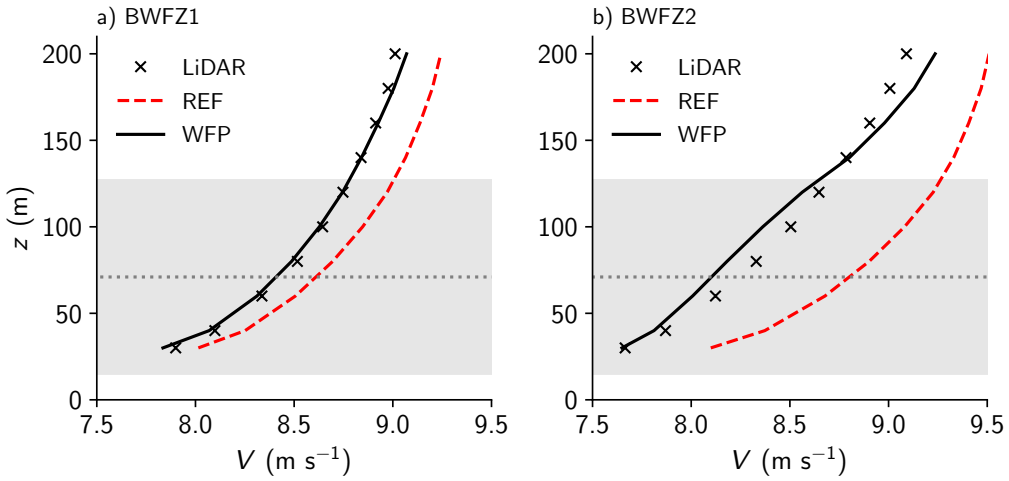

Figure 5. Vertical profiles of wind speed, from the reference run (REF) and experiment with wind-farm parameterisation (WFP), compared to the Borssele (a) BWFZ lidar 1, 10 km from the nearest wind farm and (b) BWFZ lidar 2, 2 km from the nearest wind farm. The grey dotted line indicates the mean hub height of the nearest wind farm and the grey shaded areas the area the diameter of the rotor.

the wind-farm parameterisation clearly improves the experiments; for BWFZ2, the mean profile from HARMONIE matches very well with the measurements.

6.1.2 FINO1 tower

The FINO1 tower is situated directly west of the Alpha Ventus wind farm, and north-east of the Borkum Riffgrund wind farm (Fig. 2). Fig. 6a shows the time averaged vertical wind speed profiles, compared to the corrected FINO1 measurements. In line with the results from the Borssele area, the reference simulation overestimates the wind speed with ∼0.7-0.9 m s^{-1}. With the wind-farm parameterisation included, the absolute bias is decreased, but with a slight negative bias at the highest few measurement points, ∼0.1-0.2 m s^{-1}. This underestimation seems to be partially caused by the mapping of wind turbines to the nearest HARMONIE grid point. In reality the FINO1 tower is west (and with the dominating wind direction: upstream) of the Alpha Ventus wind farm, but in HARMONIE the grid point nearest to FINO1 also houses some of the Alpha Ventus wind turbines, as shown in Fig. 6b. This means that the grid point used for the analysis, directly experiences drag from some of the Alpha Ventus turbines, resulting in a reduced wind speed. However, including the wind-farm parameterisation clearly improves the wind

297 profile at the tower location due to the many wind farms in the surroundings. This is
298 also the location where the largest impact is expected.

299 ***6.1.3 Westermost Rough lidar***

300 As shown in Fig. 4, the data availability is limited to $\sim$ 14% of the January to May
301 period, and even less at the three highest measurement heights. Therefore, the analy-
302 sis here is limited to the lowest 214 m.

303 Fig. 7 shows the time averaged vertical profiles of the lidar measurements and HAR-
304 MONIE experiments. As with the FINO1 and Borssele locations, the reference run over-
305 estimates the wind speed. The experiment with wind turbines (WFP) is very close to
306 the averaged lidar observations, especially near hub height. Above the rotor tips the gra-
307 dient at which the wind speed increases is underestimated in the model. This results in
308 a bias at 214 m of 0.2 m s^{-1} for the REF experiment and 0.3 m s^{-1} for the WFP ex-
309 periment. Since the REF experiment also underestimates the wind speed above the ro-
310 tor tip, this bias could be caused by an underestimation of the background wind speed
311 or a measured acceleration of the wind above the rotor tip not captured by HARMONIE
312 with the WFP.

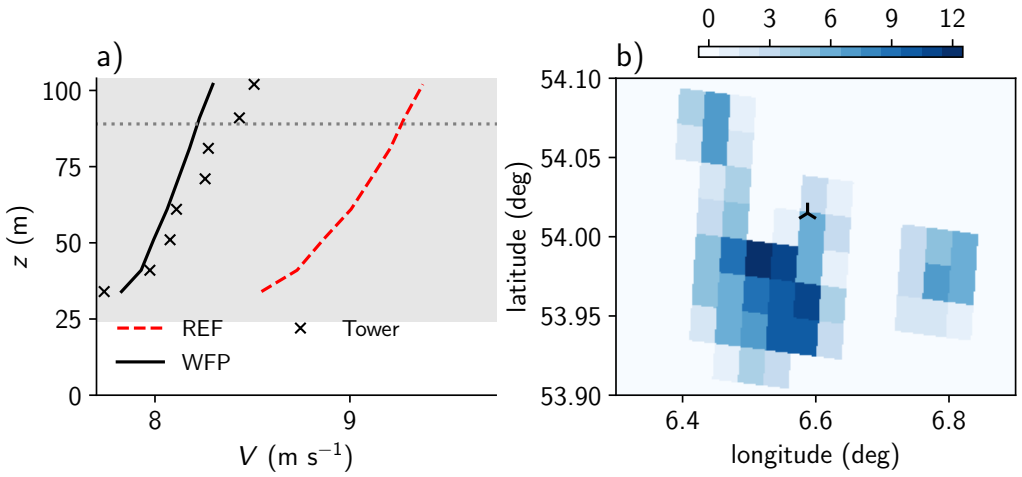

Figure 6. (a) Vertical profiles of wind speed, from the reference run without wind-farm parameterisation (REF) and experiment with wind-farm parameterisation (WFP), compared to the FINO1 tower. (b) The number of turbines in the HARMONIE grid cells surrounding FINO1

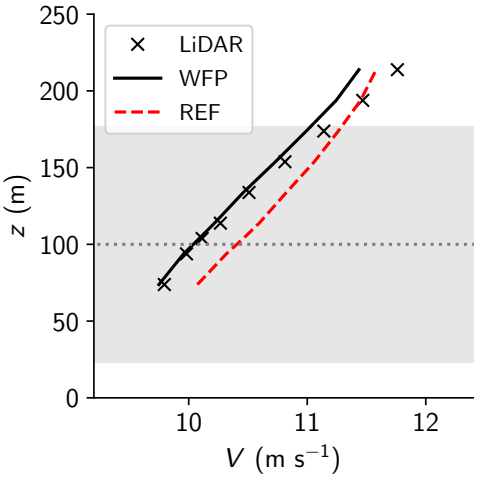

Figure 7. Vertical profiles of wind speed, from the reference run without wind-farm parameterisation (REF) and experiment with wind-farm parameterisation (WFP), compared to the Westermost rough lidar.

6.2 Airbourne measurements

For the evaluation of HARMONIE with the wind-farm parameterisation the lidar and tower measurements show significant improvements at single locations. However, in order to evaluate the spatial scale of the modelled wakes airbourne measurements are used. The WIPAFF measurement flights are intended to observe the spatial extent of the wind-farm wakes. As mentioned in sect. 5.4, we only use the airbourne measurements carried out during 6 September 2016, with a near-neutral – slightly stable surface layer and an average wind speed of 7 m s^{-1}. In those cases we expect to see a large wake from the wind farm, but not as strong as in very stable conditions (e.g. Zhan et al., 2020). Fig. 8 compares the flight measurements with the HARMONIE simulations following the same model track. For each measurement point the nearest model point in time and space was extracted for both REF and WFP simulations. The model output was interpolated between the nearest two model levels to 90 m, the flying altitude.

Close to the wind farm the wind farm wake is captured very well by the WFP (Fig. 8a). Here, at ∼4 km distance the velocity deficit is about 2 m s^{-1} and the width of the wind farm is about 15 km. During this time the background wind speed decreases left to right of the wind farm (negative to positive $x - \overline{x_{\text{turbines}}}$), however this is underestimated by the model leading to a bias of 1.0 m s^{-1} in the WFP run. An 1.5 hours later

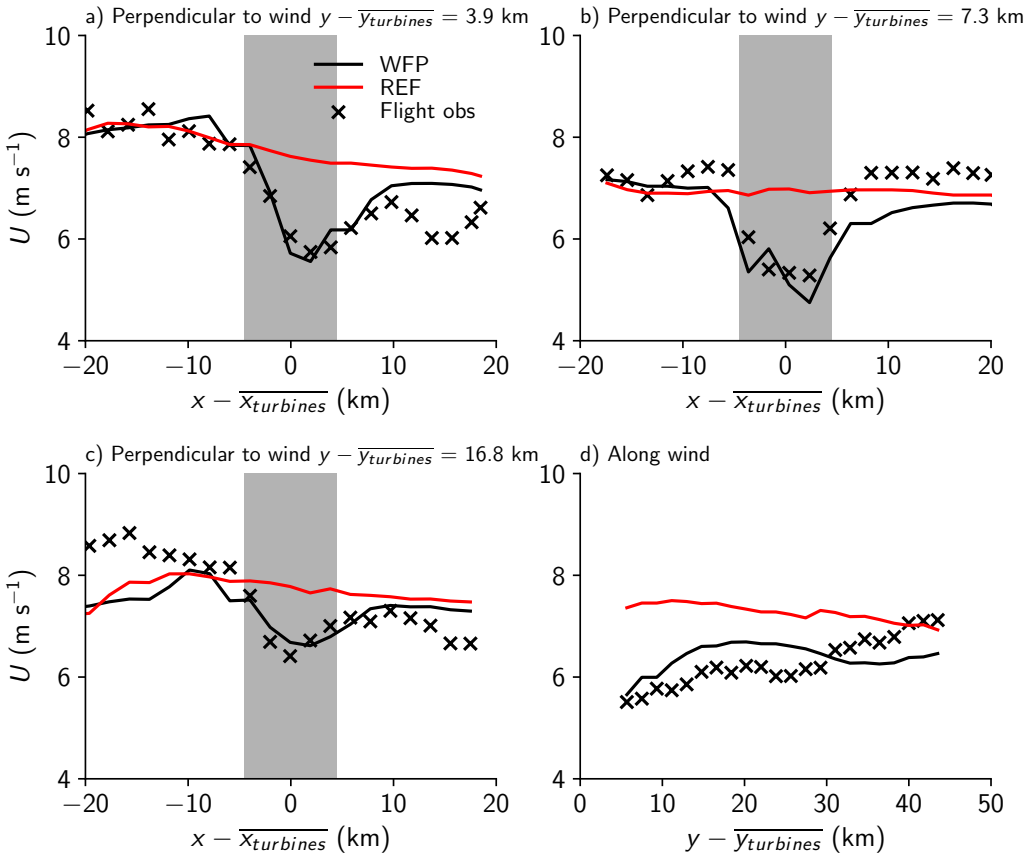

Figure 8. Cross sections through the wind farm wake of Amrumbank West in the German Bight on 6 September 2016, 12:13 – 15:20 UTC. Cross sections are perpendicular to the wind direction at (a) 3.9 km (b) 7.3 km, and (c) 16.8 km distance from the turbines, and (d) a cross section along the wind from the centre of the turbines directly downstream. Crosses indicate 60 s rolling average wind speeds at 30 s intervals from the aircraft measurements and lines indicate the interpolated modelled wind speed along the same flight path (red) reference run and (black) simulation with WFP. The grey are indicate the location of the wind farm.

(∼14:30) a cross section was taken at about 7.3 km downwind of the wind farm (Fig. 8b). Here, the HARMONIE WFP run is able to capture the wind speed in the wake of the turbines very well, but now underestimates the wind speed east of the turbines (positive $x - \overline{x_{\text{turbines}}}$)) by about 0.7 m s^{-1}. About 10 km downwind of the previous cross section (Fig. 8c), the velocity deficit in the wind-farm wake has been reduced to ∼1 m s^{-1}, captured well by in the WFP run. As expected, the REF run is unable to model the velocity deficit caused by the wind farm.

The part of the flight along the wind direction captures the recovery of the wake (Fig. 8d). About 4 km away from the wind farm the wind speed is 5.4 m s^{-1}, at 30 km away the wind speed has only increased by 0.7 m s^{-1} to 6.1 m s^{-1}. Over the same distance the model shows a similar reduction in the velocity deficit, 0.8 m s^{-1}. After 30 km the observations show the wake to dissipate quickly, while in HARMONIE there remains a difference between the REF and WFP runs of about <0.5 m s^{-1} for at least 70 km downwind of the wind farm. The Fitch et al. (2012) parameterisation is known to produce long wakes (e.g. Shepherd et al., 2020). However, a more systematic evaluation of the size and shape of wakes using Fitch et al. (2012) is needed, with more research aircraft data, scanning doppler lidars (e.g. Rhodes & Lundquist, 2013; Banta et al., 2015), or satellite measurements such as SAR (e.g. Christiansen & Hasager, 2005).

6.3 Power production

When evaluating HARMONIE with the wind-farm parameterisation, power production is a crucial quantity. Power production scales with the velocity cubed (eq. 9), making it sensitive to biases in wind speed. For all of 2016, Elia provides power production data for the Belgian offshore wind farms. This is the total power production of all the offshore wind farms. In 2016 these farms had a total capacity of 712.2 MW (Fig. 3).

Figure 9 shows the comparison between the observed power production and power production obtained from the HARMONIE experiments, both from the reference experiment and experiment with the wind turbine parameterisation (WFP). The bottom panels indicate the absolute and relative differences, averaged over 50 MW bins. The relative bias from the first (0-50 MW) bin should be treated with caution, as conditions where the observed power production equals zero result in an infinitely large relative bias.

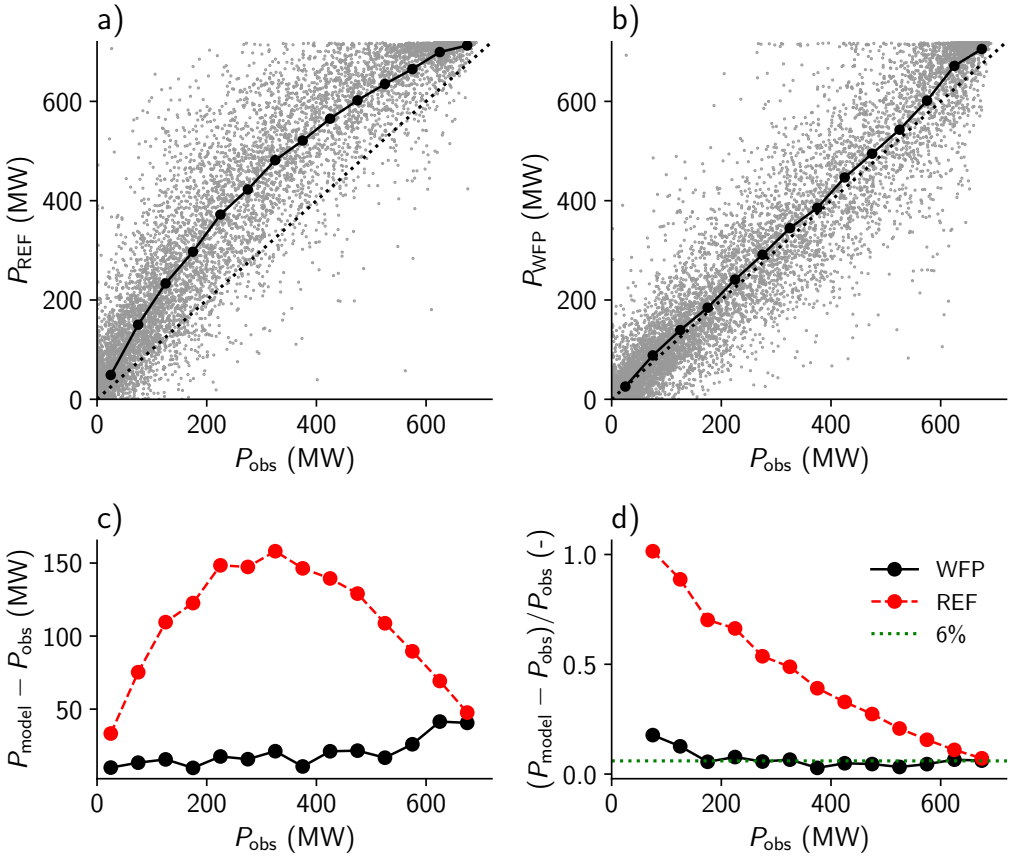

Figure 9. Power production calculated from the (a) reference reanalysis (REF) and (b) experiment with wind-farm parameterisation (WFP), compared to the Elia measurements. The solid black line with markers (top row) indicates the mean of the model data calculated over 50 MW bins. The bottom row shows the absolute (c) and relative (d) error of both model experiments.

The power production calculated offline (eq. 9) from the reference experiment clearly overestimates the production, with absolute biases as large as 150 MW, and for low wind speeds (low power production) relative biases as large as 100%. The reference simulation clearly does not include the power production losses attributed to the velocity deficit created by the wind turbines. Including the wind turbine parameterisation clearly improves the power production calculated, reducing the absolute bias to a maximum of 50 MW at high wind speeds, and the relative bias to ∼6%. There are a few possible causes for this constant relative bias – e.g. efficiency losses in the turbines or power cables, the use of (manufacturers) turbine specifications which are too optimistic, inaccuracies in the turbine parameterisation, or single turbines that are not operational, or not functioning optimally. If the aim is to deliver power production forecasts to users, some post processing will be necessary to eliminate these inaccuracies.

6.4 Impact wind farms on local meteorological conditions

As seen in the previous sections, wind turbines have an impact on the (local) wind conditions. In addition, wind turbines generate TKE, which enhances vertical mixing, potentially influencing other quantities like temperature, humidity, or clouds. Here, we briefly examine the impact of two Dutch offshore wind farms on the local meteorological conditions. In the absence of suitable measurements, the results are limited to comparing the reference simulations with the experiment including wind turbines.

Fig. 10 shows the differences in wind speed (V), potential temperature (θ), and specific humidity (q) between the experiments with and without wind turbines for two time periods. During the period March – June the sea surface temperature is colder on average compared to the atmospheric temperature and more stable cases are expected. During September – December the sea surface temperature is generally warmer than the atmosphere above, leading to more unstable cases. For each wind farm, the statistics were averaged over the HARMONIE grid points which have one or more turbines, and averaged in time.

For wind speed, the elevated drag is clearly visible, with a maximum decrease of 1.6 m s^{-1} near hub height, but a near-surface decrease of 0.3 – 0.0 m s^{-1}. The relatively small wind farm Princes Amalia (120 MW, -0.6 m s^{-1} during spring and -0.5 m s^{-1} in autumn) has a smaller impact on the wind speed compared to the larger Gemini (600

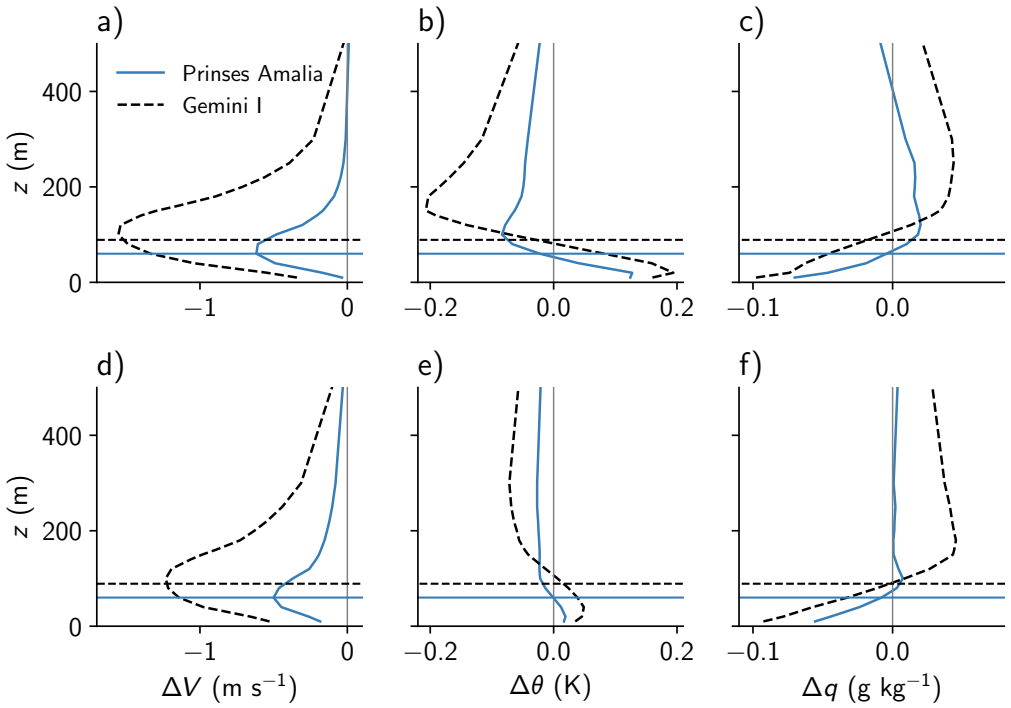

Figure 10. Impact of wind turbines on meteorological variables wind velocity (a,d), potential temperature (b,e), and specific humidity (c,f) over two Dutch offshore wind farms, Gemini to the north of the Dutch coast (black dashed) and Princes Amalia to the west of the Dutch coast (blue solid), where Δ= WFP-REF. The top panels (a – c) are averaged profiles over 1 March – 30 June 2016, the bottom panels (d – f) are averaged profiles over 1 September – 31 December 2016. The horizontal lines indicate the hub height of each wind farm.

MW, -1.6 m s^{-1} during spring and -1.2 m s^{-1} in Autumn). The modelled velocity deficit is shown to be stronger in the spring season with relatively more stable cases. Previous research has also shown higher velocity deficits during stable cases compared to unstable atmospheric boundary layers (e.g. Dörenkämper et al., 2015).

The enhanced vertical mixing has a weak impact on temperature and specific humidity. During the period where the atmosphere is on average stably stratified, the enhanced TKE and vertical mixing decreases the stratification, resulting in an increase in temperature and decrease in specific humidity near the surface, and decrease in temperature and increase in specific humidity at 100-150 m height. At the large wind farm, Gemini, this average vertical potential temperature variation is between -0.2 and 0.2 K, for the smaller wind farm (Princes Amalia) -0.08 to 0.12 K. The specific humidity during spring, decreases -0.1 for Gemini and -0.07 g kg^{-1} for Princes Amalia near the surface

and increases by 0.04 and 0.02 g kg^{-1}, respectively, above hub height. As a result of the near surface heating and drying, and the cooling and moistening aloft, the relative humidity decreases near the surface, and increases higher up. This could impact the formation of fog or low clouds.

During autumn and early winter the influence of the enhanced vertical mixing by wind turbines is smaller, for potential temperature less than 0.1 K for both wind farms. The well-mixed profiles during unstable conditions are barely influenced by enhanced TKE. However, the near-surface moisture is reduced by the same order of magnitude in the autumn compared to the spring season.

7 Conclusion

The Fitch et al. (2012) wind-farm parameterisation was implemented in mesoscale model HARMONIE-AROME, and validated with a variety of observations in the north-sea region over a one-year period. The parameterisation reduces momentum and converts this into turbulent kinetic energy and power production, depending on wind turbine properties. Two year-long simulations were performed, one including all wind turbines on the North Sea known up to 2016 and one without any wind turbines. The evaluation with various wind measurements on the North Sea indicates that inclusion of the turbine parameterisation has a positive impact on the modelled wind speeds near (offshore) wind farms. For all locations considered, the absolute bias in wind speed is decreased compared to the simulation without wind farms. Furthermore, the predicted power production – compared to observations from the Belgian TSO – shows a substantial improvement with the turbine parameterisation included.

A brief survey of the impact of wind farms on the local meteorological conditions, indicates that in addition to changes in wind speed, other quantities like temperature or humidity are influenced by wind farms as well. These variations in temperature and humidity are more pronounced in periods with more stable conditions, where the enhanced turbulent kinetic energy from the wind turbines increases the mixing of the marine boundary layer. With the expected increase in number and size of wind turbines in the coming decades the influence of wind turbines on local to regional meteorology can no longer be neglected. The relatively simple wind-farm parameterisation by Fitch et al. (2012)

improves modelled wind speed near wind farms and can be used operationally to improve weather forecasts and predicted power production.

Acknowledgments

The authors would like to acknowledge funding from the Dutch Offshore Wind Atlas (DOWA) project supported with Topsector Energy subsidy from the Ministry of Economic Affairs and Climate Policy, and the Topconsortia for Knowledge and Innovation (TKI) funded Winds of the North Sea in 2050 (WINS50) project. The authors would like to thank ECMWF for providing computational resources. We would also like to thank Jeanette Onvlee, Sukanta Basu, and Pier Siebesma for fruitfull discussions.

Data availablity

The HARMONIE-AROME model simulations are available on the KNMI data platform: https://dataplatform.knmi.nl/dataset/?tags=Dutch+Offshore+Wind+Atlas

Appendix A Wind farm and turbine information

Tables A1 and A2 provide an overview of all the wind farms implemented in the experimental domain, and Table A3 summarises the turbine types and their properties.

References

Abkar, M., & Porté-Agel, F. (2015). A new wind-farm parameterization for large-scale atmospheric models. *Journal of Renewable and Sustainable Energy*, *7*(1), 013121.

Acker, T., & Chime, A. H. (2011). Wind modeling using windpro and wasp software. *Norther Arizon University, USA*, *1560000*(8.8), 510.

Baidya Roy, S., & Traiteur, J. J. (2010). Impacts of wind farms on surface air temperatures. *Proceedings of the National Academy of Sciences*, *107*(42), 17899–17904.

Banta, R. M., Pichugina, Y. L., Brewer, W. A., Lundquist, J. K., Kelley, N. D., Sandberg, S. P., ... Weickmann, A. M. (2015). 3d volumetric analysis of wind turbine wake properties in the atmosphere using high-resolution doppler lidar. *Journal of Atmospheric and Oceanic Technology*, *32*(5), 904–914.

Name	Latitude (°N)	Longitude (°E)	Turbine type	N	Z (m)
London Array 1	51.626	1.496	SWT-3.6-120	175	87
Gemini	54.036	5.963	SWT-4.0-130	150	89
Gode Wind I	54.016	6.983	SWT-6.0-154	55	110
Gode Wind II	54.075	7.007	SWT-6.0-154	42	110
Gwynt y Mor	53.460	-3.599	SWT-3.6-107	160	98
Race Bank	53.276	0.841	SWT-6.0-154	91	110
Greater Gabbard	51.773	1.982	SWT-3.6-107	140	78
Dudgeon	53.265	1.380	SWT-6.0-154	67	110
Veja Mate	54.321	5.860	SWT-6.0-154	67	103
Anholt	56.600	11.210	SWT-3.6-120	111	82
Bard Offshore 1	54.355	5.980	BARD-5.0	80	90
GlobalTech I	54.500	6.358	Areva-5.0	80	90
Rampion Wind Farm	50.660	-0.200	V112-3.45	116	84
West of Duddon Sands	53.984	-3.464	SWT-3.6-120	108	80
Walney 1	53.810	-4.907	SWT-3.6-107	51	84
Walney 2	54.081	-3.605	SWT-3.6-107	51	90
Galloper	51.880	2.040	SWT-6.0-154	56	103
Wikinger Offshore	54.834	14.068	Adwen-5.0	70	75
Nordsee One Offshore	54.444	7.682	Senvion-6.2	54	100
Sheringham Shoal	53.135	1.147	SWT-3.6-107	88	82
Borkum Riffgrund I	53.967	6.562	SWT-4.0-12	78	87
Borkum Riffgrund II	53.967	6.496	V164-8.0	56	105
Amrumbank West	54.520	7.708	SWT-3.6-120	80	90
Thanet	51.430	1.633	V90-3.0	100	70
Nordsee Ost	54.444	7.682	Senvion-6.2	48	97
Butendiek	55.019	7.774	SWT-3.6-120	80	91
Dan Tysk	55.140	7.200	SWT-3.6-120	80	88
Baltica 2	55.070	17.100	SWT-3.6-120	80	78
Meerwind Sued/Ost	54.402	7.707	SWT-3.6-120	80	89
Sandbank	55.190	6.860	SWT-4.0-130	72	95
Lincs	53.191	0.491	SWT-3.6-120	75	100
Burbo Bank Extension	53.483	-3.273	V164-8.0	32	123
Humber Gateway	53.619	0.293	V112-3.0	73	80

Table A1. Overview of wind farms included in the experiments. Latitude and longitude indicate the location in the centre of the wind farm. N are the number of turbines in the wind farm and Z is the hub height.

Name	Latitude (°N)	Longitude (°E)	Turbine type	N	Z (m)
Westermost Rough	53.805	0.149	SWT-6.0-154	35	100
Horns Rev 2	55.600	7.582	SWT-2.3-93	91	68
Rodsand II	54.558	11.531	SWT-2.3-93	90	69
Trianel Borkum II	54.042	6.467	Areva-5.0	40	90
Kentish Flats 1	51.460	1.093	V90-3.0	30	70
Kentish Flats 2	51.450	1.079	V112-3.3	15	84
Gunfleet Sands	51.737	1.170	SWT-3.6-107	48	75
Ormonde	54.088	-3.437	Senvion-5	30	97
Barrow	53.982	-3.283	V90-3.0	30	75
Rhyl Flats	53.380	-3.646	SWT-3.6-107	25	75
North Hoyle	53.417	-3.448	V80-2.0	30	67
Riffgat	53.692	6.470	SWT-3.6-120	30	90
Horns Rev 1	55.486	7.840	V80-2.0	80	70
Nysted	54.549	11.714	SWT-2.3-82	72	69
EnBW Baltic 1	54.596	12.638	SWT-2.3-93	21	67
EOWDC	57.230	-1.990	V164-8.0	11	120
Hywind 2 Demonstration	57.500	-1.300	SWT-6.0-154	5	98
Arkonabecken Südost	54.780	14.120	SWT-6.0-154	60	102
Alpha Ventus	54.017	6.600	Avera-5.0	12	90
Walney Extension 3	54.087	-3.737	V164-8.0	40	113
Walney Extension 4	54.087	-3.737	SWT-7.0-154	47	111
Luchterduinen	52.403	4.165	V112-3.0	43	81
Prinses Amalia	52.594	4.213	V80-2.0	60	59
Egmond aan Zee	52.594	4.437	V90-3.0	36	70
Belwind I	51.670	2.800	V90-3.0	55	72
Northwind	51.619	2.901	V112-3.0	72	71
Thorntonbank	51.540	2.940	Multiple	54	95

Table A2. Table A1 continued

Name	N	P (MW)	D (m)	
Siemens SWT-2.3-82	72	2.3	72	
Siemens SWT-2.3-93	202	2.3	93	
Siemens SWT-3.6-107	563	3.6	107	
Siemens SWT-3.6-120	899	3.6	120	
Siemens SWT-4.0-120	78	4.0	120	
Siemens SWT-4.0-130	222	4.0	130	
Siemens SWT-6.0-154	478	6.0	154	(1)
Siemens SWT-7.0-154	47	7.0	154	(1)
Vestas V80-2.0	170	2.0	80	
Vestas V90-3.0	251	3.0	90	
Vestas V112-3.0	188	3.0	112	
Vestas V112-3.3	15	3.3	112	
Vestas V112-3.45	116	3.45	112	
Vestas V164-8.0	139	8.0	164	(2)
Senvion 5	30	5.0	126	
Senvion 6.2	156	6.2	126	
BARD-5.0	80	5.0	126	(3)
Adwen-5.0	202	5.0	116	(3)
Haliade-6	1	6.0	100	
	3908	460×10^3		

Table A3. Overview of the wind turbine types included in the experiments. The total installed power equals $\sum N \times P$. Notes: (1) replaced with 6 MW reference turbine from (Bulder et al., 2016), (2) replaced with 8 MW reference turbine from (Bulder et al., 2016), (3) replaced with Senvion 5 turbine.

Bärfuss, K., Hankers, R., Bitter, M., Feuerle, T., Schulz, H., Rausch, T., ... Lampert, A. (2019). In-situ airborne measurements of atmospheric and sea surface parameters related to offshore wind parks in the german bight. *PANGAEA https://doi. org/10.1594/PANGAEA*, *902845*.

Bengtsson, L., Andrae, U., Aspelien, T., Batrak, Y., Calvo, J., de Rooy, W., ... others (2017). The HARMONIE–AROME model configuration in the ALADIN–HIRLAM NWP system. *Monthly Weather Review*, *145*(5), 1919–1935.

Bulder, B., Bot, E., & Marina, A. (2016). *Scoping analysis of the potential yield of the Hollandse Kust (zuid) wind farm sites and the influence on the existing wind farms in the proximity* (Tech. Rep. No. ECN-E-16-021 - 2nd edt.) ECN.

Christiansen, M. B., & Hasager, C. B. (2005). Wake effects of large offshore wind farms identified from satellite sar. *Remote Sensing of Environment*, *98*(2-3), 251–268.

de Haan, S. (2011). High-resolution wind and temperature observations from aircraft tracked by Mode-S air traffic control radar. *Journal of Geophysical Research:*

Atmospheres, *116*(D10).

de Haan, S. (2016). Estimates of Mode-S EHS aircraft-derived wind observation errors using triple collocation. *Atmospheric Measurement Techniques*, *9*(8), 4141–4150.

de Rooy, W. C., Siebesma, P., Baas, P., Lenderink, G., de Roode, S., de Vries, H., ... van 't Veen, B. (2021). Model development in practice: A comprehensive update to the boundary layer schemes in HARMONIE-AROME. *Geoscientific Model Development*, -(-), –.

Dörenkämper, M., Witha, B., Steinfeld, G., Heinemann, D., & Kühn, M. (2015). The impact of stable atmospheric boundary layers on wind-turbine wakes within offshore wind farms. *Journal of Wind Engineering and Industrial Aerodynamics*, *144*, 146–153.

Duncan, J. B., Wijnant, I. L., & Knoop, S. (2019). *DOWA validation against offshore mast and LiDAR measurements.* (Tech. Rep. No. TNO Technical Report 2019 R10062). Retrieved from `https://www.dutchoffshorewindatlas.nl/publications/reports/2019/05/21/tno-report-dowa-validation-against-offshore-mast-and-lidar-measurements`

Faroux, S., Kaptué Tchuenté, A., Roujean, J.-L., Masson, V., Martin, E., & Moigne, P. L. (2013). Ecoclimap-ii/europe: A twofold database of ecosystems and surface parameters at 1 km resolution based on satellite information for use in land surface, meteorological and climate models. *Geoscientific Model Development*, *6*(2), 563–582.

Fischer, C., Montmerle, T., Berre, L., Auger, L., & Ştefănescu, S. E. (2005). An overview of the variational assimilation in the ALADIN/France numerical weather-prediction system. *Quarterly Journal of the Royal Meteorological Society*, *131*(613), 3477–3492.

Fischereit, J., Brown, R., Larsén, X. G., Badger, J., & Hawkes, G. (2021). Review of mesoscale wind-farm parametrizations and their applications. *Boundary-Layer Meteorology*, 1–50.

Fitch, A. C., Olson, J. B., Lundquist, J. K., Dudhia, J., Gupta, A. K., Michalakes, J., & Barstad, I. (2012). Local and mesoscale impacts of wind farms as parameterized in a mesoscale NWP model. *Monthly Weather Review*, *140*(9), 3017–3038.

Gustafsson, N., Janjić, T., Schraff, C., Leuenberger, D., Weissmann, M., Reich, H., ... others (2018). Survey of data assimilation methods for convective-scale numerical weather prediction at operational centres. *Quarterly Journal of the Royal Meteorological Society*, *144*(713), 1218–1256.

Hersbach, H., Bell, B., Berrisford, P., Hirahara, S., Horányi, A., Muñoz-Sabater, J., ... others (2020). The era5 global reanalysis. *Quarterly Journal of the Royal Meteorological Society*, *146*(730), 1999–2049.

Lampert, A., Bärfuss, K., Platis, A., Siedersleben, S., Djath, B., Cañadillas, B., ... others (2020). In situ airborne measurements of atmospheric and sea surface parameters related to offshore wind parks in the german bight. *Earth System Science Data*, *12*(2), 935–946.

Lampert, A., Bärfuss, K., Platis, A., Siedersleben, S., Djath, B., Cañadillas, B., ... Emeis, S. (2020). In situ airborne measurements of atmospheric and sea surface parameters related to offshore wind parks in the german bight. *Earth System Science Data*, *12*(2), 935–946. Retrieved from `https://essd.copernicus.org/articles/12/935/2020/` doi: 10.5194/essd-12-935-2020

Lee, J. C., & Lundquist, J. K. (2017). Evaluation of the wind farm parameterization in the weather research and forecasting model (version 3.8. 1) with meteorological and turbine power data. *Geoscientific Model Development*, *10*(11), 4229–4244.

Lenderink, G., & Holtslag, A. A. (2004). An updated length-scale formulation for turbulent mixing in clear and cloudy boundary layers. *Quarterly Journal of the Royal Meteorological Society: A journal of the atmospheric sciences, applied meteorology and physical oceanography*, *130*(604), 3405–3427.

Marseille, G.-J., & Stoffelen, A. (2017). Toward scatterometer winds assimilation in the mesoscale harmonie model. *IEEE Journal of Selected Topics in Applied Earth Observations and Remote Sensing*, *10*(5), 2383–2393.

Martín Míguez, B., Novellino, A., Vinci, M., Claus, S., Calewaert, J.-B., Vallius, H., ... others (2019). The european marine observation and data network (emodnet): visions and roles of the gateway to marine data in europe. *Frontiers in Marine Science*, *6*, 313.

Masson, V., Le Moigne, P., Martin, E., Faroux, S., Alias, A., Alkama, R., ... oth-

ers (2013). The surfexv7. 2 land and ocean surface platform for coupled or offline simulation of earth surface variables and fluxes. *Geoscientific Model Development*, *6*(4), 929–960.

Muñoz-Esparza, D., Cañadillas, B., Neumann, T., & Van Beeck, J. (2012). Turbulent fluxes, stability and shear in the offshore environment: Mesoscale modelling and field observations at fino1. *Journal of Renewable and Sustainable Energy*, *4*(6), 063136.

Platis, A., Bange, J., Bärfuss, K., Cañadillas, B., Hundhausen, M., Djath, B., ... others (2020). Long-range modifications of the wind field by offshore wind parks–results of the project wipaff. *Meteorologische Zeitschrift*, 355–376.

Platis, A., Hundhausen, M., Mauz, M., Siedersleben, S., Lampert, A., Bärfuss, K., ... others (2021). Evaluation of a simple analytical model for offshore wind farm wake recovery by in situ data and weather research and forecasting simulations. *Wind Energy*, *24*(3), 212–228.

Rhodes, M. E., & Lundquist, J. K. (2013). The effect of wind-turbine wakes on summertime us midwest atmospheric wind profiles as observed with ground-based doppler lidar. *Boundary-layer meteorology*, *149*(1), 85–103.

Shepherd, T., Barthelmie, R., & Pryor, S. (2020). Sensitivity of wind turbine array downstream effects to the parameterization used in wrf. *Journal of Applied Meteorology and Climatology*, *59*(3), 333–361.

Skamarock, W. C., Klemp, J. B., Dudhia, J., Gill, D. O., Liu, Z., Berner, J., ... others (2019). A description of the advanced research wrf model version 4. *National Center for Atmospheric Research: Boulder, CO, USA*, 145.

Volker, P., Badger, J., Hahmann, A. N., & Ott, S. (2015). The explicit wake parametrisation v1. 0: a wind farm parametrisation in the mesoscale model wrf. *Geoscientific Model Development*, *8*(11), 3715–3731.

Wagner, D., Steinfeld, G., Witha, B., Wurps, H., & Reuder, J. (2019). Low level jets over the southern north sea. *Meteorologische Zeitschrift*, 389–415.

Westerhellweg, A., Canadillas, B., Beeken, A., & Neumann, T. (2010). One year of lidar measurements at fino1-platform: Comparison and verification to mast data. In *Proceedings of 10th german wind energy conference dewek* (pp. 1–5).

Westerhellweg, A., Neumann, T., & Riedel, V. (2012). Fino1 mast correction.

DEWI-Magazin, *21*.

Wijnant, I. L., van Ulft, B., van Stratum, B. J. H., Barkmeijer, J., Onvlee, J., de Valk, S., C. Knoop, ... Klein Baltink, H. (2019). *The dutch offshore wind atlas (DOWA): description of the dataset* (Tech. Rep.). Retrieved from `https://www.dutchoffshorewindatlas.nl/publications`

WindEurope. (2017). *Wind energy in europe: Scenarios for 2030* (Tech. Rep.). Retrieved from `https://windeurope.org/wp-content/uploads/files/about-wind/reports/Wind-energy-in-Europe-Scenarios-for-2030.pdf`

Witkin, A. P., & Heckbert, P. S. (2005). Using particles to sample and control implicit surfaces. In *Acm siggraph 2005 courses* (p. 260).

Wu, C., Luo, K., Wang, Q., & Fan, J. (2022). A refined wind farm parameterization for the weather research and forecasting model. *Applied Energy*, *306*, 118082.

Zhan, L., Letizia, S., & Valerio Iungo, G. (2020). Lidar measurements for an onshore wind farm: Wake variability for different incoming wind speeds and atmospheric stability regimes. *Wind Energy*, *23*(3), 501–527.